Excited electron transfer between a core-excited $Ar^*(2p_{3/2}^{-1}4s)$ atom and the metal substrate in the Ar/Cu(111) system

J. P. Gauyacq and A. G. Borisov
Laboratoire des Collisions Atomiques et Moléculaires, Unité Mixte de Recherche CNRS–Université Paris Sud UMR 8625, Bâtiment 351, Université Paris-Sud, 91405 Orsay Cedex, France
(Received 13 January 2004; published 22 June 2004)

The transfer of the excited electron from the core-excited $Ar^*(2p_{3/2}^{-1}4s)$ atom to a metal substrate is studied theoretically in the case of Ar atoms physisorbed on Cu(111). The study is based on a wave packet propagation (WPP) approach associated with a model representation of the system. The *L* band gap of Cu is shown to lead to a drastic decrease of the resonant charge transfer rate in the case of a Cu(111) surface, as compared to the case of a free-electron metal surface. Comparison between the present results and earlier results for the charge transfer rates in alkali/Cu(111) systems allows a discussion of the validity of the so-called $Z+1$ approximation for core-excited states. The cases of a single Ar atom and of 1, 2, and 3 monolayers of Ar on the surface are investigated. The dynamics of the excited electron transfer is shown to be strongly influenced by neighboring Ar atoms, through polarization and confinement effects associated with the insulating properties of solid Ar. The present theoretical results are discussed in connection with recent experimental results on the Ar*-metal charge transfer problem.

DOI: 10.1103/PhysRevB.69.235408 PACS number(s): 73.20.Hb, 34.70.+e, 73.40.Gk, 77.55.+f

I. INTRODUCTION

The x-ray absorption spectrum of atoms presents a series of resonances located below the ionization threshold of inner shells that correspond to the excitation of an inner shell electron to a vacant outer orbital. Such a core-excited atomic state can relax via autoionization, the outer excited electron being a spectator. The complete process, x-ray absorption +autoionization, is usually described as an Auger resonant Raman scattering process.[1,2] In the case of an atom adsorbed on a metal surface, another deexcitation channel can exist associated with the transfer of the excited outer electron into the metal. After the electron transfer, the adsorbate has become a positive ion with an inner vacancy and decays via Auger emission. In the case of an adsorbed atom, one then has two distinct decay channels for the core-excited state, which compete with each other and can be separated experimentally. For example, the core-excited Ar atom studied in the present work, $Ar^*(2p_{3/2}^{-1}4s)$, corresponding to the excitation of a $2p_{3/2}$ core electron to the outer 4*s* orbital, can decay along two different schemes when Ar is adsorbed on a metal surface, the $2p$ hole relaxing before or after the transfer of the 4*s* electron into the metal. The existence of the two decay schemes has been evidenced experimentally via the study of the emitted electron spectra, and their branching ratio has been determined. It has then be proposed to use this branching ratio to determine the characteristic time for electron transfer between an adsorbate and a metal surface,[3–8] supposing that the core hole lifetime, which is known from linewidth measurements in free atoms, is not influenced by the presence of the spectator excited electron nor by that of the neighboring metal surface. This method has been named the "core hole clock" method. It can efficiently compete with direct time measurement of charge transfer times using pump-probe experiments with femtosecond lasers in adsorbate/substrate systems.[9] For the $Ar^*(2p_{3/2}^{-1}4s)$ state, the core hole lifetime has been determined to be around 6 fs,[10] which is then quite appropriate to determine adsorbate-substrate electron transfer times. The core hole clock method has been applied to a few different systems, and in particular to the $Ar^*(2p_{3/2}^{-1}4s)$ excited state in the case of Ar layers adsorbed on various metal substrates.[6–8,11–14]

The electron transfer between an atom and a metal surface has received a lot of attention in various contexts: collisional charge transfer, resonance mediated reaction mechanisms at surfaces, and lifetime of excited states at surfaces, and it is now rather well understood for simple systems. When energetically possible, the resonant electron transfer between an atom and a metal surface is the most efficient process. It is a one-electron energy-conserving process, in which the electron tunnels through the potential barrier separating the atom and the metal.[15] Nonperturbative treatments of the resonant charge transfer process (RCT) process are now available[16–21] that can accurately account for experimental findings in simple systems.[22–24] On a free-electron metal, for an atom sitting at a typical adsorption distance, the RCT process is very fast, occurring on a time scale of a fraction of a femtosecond. This makes excited states (with the excited electron energy above the Fermi level) very short lived. This is, for example, the case of alkali metal atoms on free-electron metals.[23,25]

The RCT efficiency appears to be severely weakened on certain metal surfaces, where very long-lived adsorbate-localized excited states have been observed. For example, in the case of Cs adsorbates on a Cu(111) surface, lifetimes of a few tens of femtoseconds have been reported[26–28] in contrast to the subfemtosecond lifetime expected on a free-electron metal substrate.[23,25] This observation is very important for the prospect of excited state mediated reaction processes at surfaces, where usually a too short lifetime is a bottleneck for the reaction. Consistently, Cs desorption has been shown to result from laser excitation of Cs adsorbates.[29] The block-

ing of the RCT in Cs/Cu(111) has been attributed to the existence of the Cu *L* band gap in the direction normal to the (111) surface, which forbids electron propagation along the surface normal at the energy of the Cs resonant state.[30] This phenomenon has been described theoretically in detail, allowing one to account for the experimental observations, including the Cs desorption.[30–33] In particular, it has been shown that when the RCT process is not energetically possible or is hindered by a band gap, then multielectron charge transfer processes play a role.[31] These processes correspond to the inelastic interaction of the excited electron with the substrate electrons, the extra energy being transferred to a substrate electron or to a plasmon, a collective excitation of the substrate electron gas.[34,35]

An excited atom, such as $Ar^*(2p_{3/2}^{-1}4s)$ has the structure of a compact ionic core with an outer excited electron around it. Very often, such excited states have been described using the so-called $Z+1$ approximation, in which the core-excited state of the atom is compared to a low-lying state of the next atom in the periodic table. Within this $Z+1$ approximation, $Ar^*(2p_{3/2}^{-1}4s)$ looks like K(4*s*) (see, e.g., in Ref. 8). One can then predict properties of the core-excited Ar states from the knowledge of the "simpler" potassium atom. Equivalently, one could also use studies of the $Ar^*(2p_{3/2}^{-1}4s)$ state to get information on the K(4*s*) level. This last scheme has been used to discuss the nature of the bonding of a K adsorbate with a graphite surface[5,36] and confirmed the ionic nature of this bond in the case of the disperse phase of K/graphite. Based on the $Z+1$ approximation and on the above-mentioned results on alkali metal adsorbates, one can expect the electron transfer rate between a core-excited rare gas atom and a metal to be significantly influenced by the presence of a projected band gap on the surface. The aim of the present paper is to study this problem on the example of the core-excited $Ar^*(2p_{3/2}^{-1}4s)$ state on a Cu(111) metal surface. Since the 4*s* electron lies in the Cu *L* band gap, we compare results obtained with a free-electron substrate and Cu(111) to illustrate the projected band gap effect. Direct comparison between the present results and earlier results for K adsorbates[32] allows us to qualitatively and quantitatively test the $Z+1$ approximation. We examine both the case of a single Ar adsorbate on the metal and the case of core-excited $Ar^*(2p_{3/2}^{-1}4s)$ inside complete Ar layers on metal substrates. This illustrates the effect of the Ar neighbors on the energy of the $Ar^*(2p_{3/2}^{-1}4s)$ state and on the dynamics of the RCT, as well as the effect of the geometric position of the excited Ar atom inside a multilayer system.

Below, Sec. II presents the theoretical approaches used in the present work. Section III is devoted to the results for the $Ar^*(2p_{3/2}^{-1}4s)$ state in the case of a single Ar adsorbate on a metal surface, and Sec. IV to the results in the case of Ar multilayers. Both the Cu(111) substrate and a free-electron metal substrate are considered. Section V discusses the present results and their relation to earlier experimental studies, and Sec. VI summarizes the main findings of this work.

II. METHOD

The dynamics of the charge transfer between a core-excited $Ar^*(2p_{3/2}^{-1}4s)$ atom and a metal surface is studied using a one-electron three-dimensional wave packet propagation (WPP) method. It consists in studying the time evolution of the 4*s* outer electron in the $Ar^*(2p_{3/2}^{-1}4s)$ state, the Ar^+ excited core being a spectator. In such an approach, the decay of the Ar* state is entirely due to the atom-surface charge transfer and thus the level width yields the charge transfer rate. The application of the WPP method to the atom-surface charge transfer has already been presented in detail in Refs. 18 and 37 for its two-dimensional (2D) version and it is only briefly discussed below, with emphasis on the specificity of the present 3D study. Several preliminary calculations were also performed using the coupled angular mode (CAM) method;[17,38] their results are briefly presented in Sec. III as a test of the present Ar* description.

The interaction of the outer electron in the $Ar^*(2p_{3/2}^{-1}4s)$ state with the various parts of the system is described via the following Hamiltonian H:

$$H = T + V_{e\text{-surf}} + V_{e-Ar^+\ \text{core}} + V_{e-Ar^+\ \text{image}} + V_{e-Ar\ \text{layer}} - iV_{ee} \tag{1}$$

where T is the electron kinetic energy, $V_{e\text{-surf}}$ is the interaction of the electron with the clean metal surface, $V_{e-Ar^+\ \text{core}}$ is the interaction between the electron and the Ar^+ core, $V_{e-Ar^+\ \text{image}}$ is the interaction of the electron with the image of the Ar^+ ion core, $V_{e-Ar\ \text{layer}}$ is the interaction between the electron and the adsorbed Ar layer, and V_{ee} is an effective representation of the inelastic electron-electron interaction.

A. Description of the potentials

The interaction of the electron with the clean metal surface, $V_{e\text{-surf}}$, is described by a local potential, that is assumed to depend only on z, the electron-surface distance, i.e., the electron motion parallel to the surface is assumed to be free. Two model representations were used. For a free-electron metal surface, we used the potential from Jennings *et al.*[39] and for the Cu(111) surface we used the model potential obtained in Ref. 40 from an *ab initio* density functional theory study. The latter represents quite well the specificities of the electron motion perpendicular to the surface (position of the projected *L* band gap, position of the image, and surface states).

The pseudopotential $V_{e-Ar^+\ \text{core}}$ is of the Kleinman-Bylander form[41] and it was built from an ℓ-dependent pseudopotential V_ℓ. The interaction between the Ar^+ core angular momentum and the outer electron momentum is neglected, and thus V_ℓ is taken as an ℓ-dependent central potential, a function of r, the electron-Ar^+ distance. V_ℓ is chosen of the same form as the pseudopotentials introduced by Bardsley for the alkalis metals:[42]

$$V_\ell = -\frac{1}{r} - 0.5\frac{\alpha_d}{(r^2+d^2)} - 0.5\frac{\alpha_q}{(r^2+d^2)^2} + A_\ell \exp(-B_\ell r^2). \tag{2}$$

α_d and α_q are the Ar^+ core polarizabilities; they were taken equal to those for K^+ in Ref. 42 (5.47 and 41.5 a.u., respectively), as well as the cutoff radius d (1.5 a.u.). The coefficients A_ℓ and B_ℓ (for $\ell=0$, 1, and 2) are given in Table I.

TABLE I. Values in atomic units of the A_ℓ and B_ℓ parameters for the pseudopotential describing the core-excited $Ar^*(2p_{3/2}^{-1}n\ell)$ free atom [Eq. (2)].

ℓ	A_ℓ	B_ℓ
0	9.119826	0.668557
1	2.905684	0.343892
2	−4.314704	0.738756

They were determined by adjustment to reproduce the binding energy of the outer electron in the $Ar^*(2p_{3/2}^{-1}n\ell)$ states, as they have been determined experimentally for the free atom.[43,44] For ℓ greater than or equal to 3, V_ℓ was taken equal to V_0. From the V_ℓ pseudopotentials, we built the Kleinman-Bylander form pseudopotentials:

$$V_{e-\mathrm{Ar}^+\ \mathrm{core}} = V_0(r) + V_{\mathrm{NL}}(\vec{r}). \tag{3}$$

The nonlocal part of the potential (3) is given by

$$V_{\mathrm{NL}}(\vec{r}) = \sum_{\ell=1,2;m} \frac{|\phi_\ell^m \Delta V_\ell\rangle\langle \Delta V_\ell \phi_\ell^m|}{\langle \phi_\ell^m|\Delta V_l|\phi_\ell^m\rangle}\delta_{m,0}, \tag{4}$$

where $\Delta V_\ell = (V_\ell - V_0)$ and ϕ_ℓ^m are the wave functions of the $4p$ and $3d$ orbitals (m is the projection of the outer electron angular momentum on the quantization axis z). The z axis is chosen here as the normal to the surface going through the Ar* center. The development over ℓ, m terms in Eq. (4) is limited to $m=0$ terms due to the symmetry of the present system. Indeed, in the free atom, the $4s$ orbital of the $Ar^*(2p_{3/2}^{-1}4s)$ atom corresponds to $m=0$. For a single atom on the surface, m is still a good quantum number. The z axis is a sixfold symmetry axis for a single Ar monolayer on the surface and a threefold symmetry axis for a thicker layer. As a consequence, in the Ar layer case, the $m=0$ states are coupled to $m=\pm 6$ or $m=\pm 3$ states, depending on the layer thickness. This involves terms with at least $\ell=6$ (3) in the atomic pseudopotential (4) for which ΔV_ℓ vanishes.

$V_{e-\mathrm{Ar}^+\ \mathrm{image}}$ describes the modification of the electron-surface interaction potential due to the presence of the charged Ar^+ ion core, i.e., induced by the screening of the ion core charge by the metal. $V_{e-\mathrm{Ar}^+\ \mathrm{image}}$ is described using a classical point charge image of the Ar^+ core.

The $V_{e-\mathrm{Ar\ layer}}$ potential is present only when we consider that more than one Ar atom is adsorbed on the surface. This potential has been built in the same way as the pseudopotential used in the study of image states on Ar/Cu surfaces.[45,46] The 1 monolayer (ML) Ar lattice on Cu(111) is assumed to be hexagonal and incommensurate with the Cu lattice as for the[47] Cu(110) and[45,46] (100) surfaces, with a surface density slightly lower than that of a bulk (111) plane. Only the adsorption distance and surface density play a role in the present study and they have been taken equal to those for a Cu(100) surface,[46] i.e., $6.94a_0$ for 1 ML adsorption height measured from the last Cu plane and $7.52a_0$ for the nearest neighbor distances within each layer. For building the $V_{e-\mathrm{Ar\ layer}}$ potential, we used a local potential to describe the interaction between an electron and a free Ar atom, defined as the sum of a short-range potential and a long-range polarization potential.[46] This local potential has been adjusted in Ref. 46 to represent the low energy scattering of electrons by a free Ar. This potential supports two core levels of s and p symmetry that mimic the effect of the orthogonality of the $e-$Ar scattering wave function to the $3s$ and $3p$ occupied orbitals of the Ar target. The contributions from the various Ar atoms to the $V_{e-\mathrm{Ar\ layer}}$ potential are then added with proper care of the mutual polarization of the Ar atoms (see Ref. 46 for details). This procedure ensures that the proper dielectric properties of the Ar layer on the metal surface are accounted for. It has been shown to be successful in representing the electronic structure of bulk Ar at low energy as well as the dynamics of the image state electrons in the Ar/Cu(100) system.[45,46] The convergence of the interaction potential between the electron and an adsorbed Ar layer requires including a large number of Ar atoms in the layer. This is particularly true for an electron far away from the layer, when the system reduces to the polarization of the Ar layer by the Ar^+ ion core. However, in the present case, the $4s$ orbital is localized around the Ar^+ ion core and is mainly perturbed by the first Ar neighbors in the layer. So the convergence of the properties of the Ar* state (energy and RCT rate) can be reached with a limited number of atoms in the layer (see the discussion below).

The complex potential $(-iV_{ee})$ is introduced in some of the calculations reported below in order to represent the inelastic scattering of the active electron by the Cu bulk electrons. Indeed, the present study, based on the Hamiltonian (1), is monoelectronic and only considers the active electron, i.e., the $4s$ electron of the core-excited Ar* atom. In the case of a free-electron metal surface, the RCT process is extremely fast and a monoelectronic study can quantitatively account for the excited state decay. However, if the RCT decay rate Γ_{RCT} is much reduced, as, e.g., by a projected band gap, then the effect of weaker interactions has to be considered. The multielectron interactions have been shown to play an important role in the excited state decay in such situations (see, e.g., the discussion in Ref. 32). In the present work, following approaches developed in low energy electron diffraction studies,[48] we represent these interactions by an effective complex potential $(-iV_{ee})$ localized inside the metal. *A priori*, the effect of the electron-electron inelastic interactions depends on the excited state energy (see Ref. 49 and references therein). To account for this variation we assumed that V_{ee} takes the form

$$V_{ee} = C(E_{\mathrm{res}} - E_F)^2 \tag{5}$$

where E_{res} is the energy of the state under study, and E_F is the Fermi energy. C is a constant that has been adjusted on the Cs/Cu(111) system so that the WPP calculations with the complex potential [Eq. (5)] reproduce the *ab initio* results[32] for the many body contribution to the population decay rate of the adsorbate induced state in the Cs/Cu(111) system. In practice, this leads to $C=0.007\ 98\ \mathrm{eV}^{-1}$. Tests on the present system have shown that the total $4s$ decay rate varies like $\Gamma_{\mathrm{RCT}}+aC$, when C is varied, confirming the independence of the two contributions to the $4s$ decay in our approach. One can also stress that the RCT process is strongly dominating

the charge transfer in the present system (see below) so that the inaccuracies introduced by the use of an effective representation of the multielectron contribution to the Ar*-surface charge transfer should not significantly influence the final results.

B. Wave packet propagation

The WPP approach consists in solving the 3D time-dependent Schrödinger equation with the Hamiltonian (1) on a grid of points. The initial condition $\Psi(\vec{r},t=0)=\Phi_0(\vec{r})$ corresponds to the 4*s* orbital in the free atom, thus ensuring a good overlap between the wave packet and the resonant state in the Ar/Cu system. The wave packet is written in cylindrical coordinates (ρ,ϕ,z), well adapted to the symmetry of the problem. The *z* axis is normal to the surface and goes through the center of the core-excited Ar* atom. Typically, the grid involves $350\times64\times512$ points. The time propagation of the wave packet is performed using the split-operator technique,[50,51] following

$$\Psi(t+dt)=\exp(-iHdt)\Psi(t) = e^{-iVdt/2}\mathcal{F}^{-1}_{m\to\phi}e^{-i\tilde{H}\,dt}\mathcal{F}_{\phi\to m}e^{-iVdt/2}\Psi(t)+O(dt^3). \tag{6}$$

V is the local part of the potential:

$$V=V_0+V_{e\text{-surf}}+V_{e-\mathrm{Ar}^+\ \text{image}}+V_{e-\text{Ar layer}}-iV_{ee} \tag{7}$$

and the Hamiltonian $\tilde{H}$ is given by

$$\tilde{H}=T_z+T_\rho+V_{NL}=-\frac{1}{2}\frac{d^2}{dz^2}-\frac{1}{2}\frac{1}{\rho}\frac{d}{d\rho}\rho\frac{d}{d\rho}+\frac{m^2}{2\rho^2}+V_{NL}. \tag{8}$$

We used the pseudospectral approach[51,52] with fast Fourier transform ($\mathcal{F}$) to switch between the ϕ and *m* representations of the wave function:

$$\Psi_m(\rho,z;t)=\mathcal{F}_{\phi\to m}\{\Psi(\rho,\phi,z;t)\} =\frac{1}{\sqrt{N_\phi}}\sum_{j=0}^{N_\phi-1}\Psi(\rho,\phi_j,z;t)e^{-i2\pi jk/N_\phi},$$

$$k=-N_\phi/2,\ldots,N_\phi/2-1. \tag{9}$$

Here, $m=kI_S$, where I_S is the order of the symmetry of the *z* axis. N_ϕ is the total number of ϕ points in the mesh, and $\phi_j=2\pi j/N_\phi I_S$.

In Eq. (6), $\mathcal{F}^{-1}_{m\to\phi}$ stands for the inverse Fourier transform from *m* to ϕ representations.

The $e^{-i\tilde{H}\,dt}$ term is evaluated through a further split-operator procedure:

$$e^{-i\tilde{H}\,dt}=e^{-iV_{NL}dt/2}e^{-iT_zdt/2}e^{-iT_\rho dt}e^{-iT_zdt/2}e^{-iV_{NL}dt/2}. \tag{10}$$

Coordinate mapping is used for the ρ coordinate, and a finite difference scheme together with Cayley transform is used to calculate the action of the $e^{-iT_\rho dt}$ operator (see details in Refs. 37 and 53). The pseudospectral approach associated with a uniform mesh ($\Delta z=0.5a_0$) and a fast Fourier transform is used to calculate the action of the e^{-iT_zdt} operator. The action of the nonlocal part of the potential is given by

$$e^{-iV_{NL}dt/2}=1+\sum_{\ell=1,2}\delta_{m,0}\frac{1}{(\Delta V_\ell^2)_{\ell\ell}}\left[\exp\left(-i\frac{dt}{2}\frac{(\Delta V_\ell^2)_{\ell\ell}}{(\Delta V_\ell)_{\ell\ell}}\right)-1\right] \times|\phi_\ell^m\Delta V_\ell\rangle\langle\Delta V_\ell\phi_\ell^m|, \tag{11}$$

where $(\Delta V_\ell^2)_{\ell\ell}=\langle\phi_\ell^0|(\Delta V_\ell)^2|\phi_\ell^0\rangle$ and $(\Delta V_\ell)_{\ell\ell}=\langle\phi_l^0|\Delta V_\ell|\phi_\ell^0\rangle$.

Finally, to avoid artificial reflections of the wave packet an absorbing potential is introduced at the grid boundaries. The typical time step of the propagation is equal to 0.1 a.u.

From the time-dependent wave packet, we get the survival amplitude of the electron in the initial state:

$$A(t)=\langle\Phi_0(\vec{r})|\Psi(\vec{r},t)\rangle \tag{12}$$

from which the system density of states (DOS) projected on Φ_0 can be extracted via a Laplace transform.[37] Peaks appear in the projected DOS at the location of the excited states of the system, and the width of the peak yields the decay rate of the excited state in the given calculation. Alternatively, a fit of the $A(t)$ time dependence yields the energy and width of the resonances of the system (see Ref. 37 for details). If the Hamiltonian is the one given by Eq. (1), then the decay rate corresponds to the sum of the decay rate via RCT and via inelastic electron-electron interactions, i.e., the total 4*s* decay rate. If the V_{ee} term is omitted, only the RCT decay rate is obtained. In both cases, the decay rate of the inner hole of the core-excited Ar* state is not included, so that these decay rates are not the inverse of the state lifetime, but rather the inverse of the 4*s* electron lifetime against charge transfer into the metal.

III. SINGLE Ar ATOM ON A METAL SUBSTRATE

We first discuss the properties of a single Ar atom in the $(2p_{3/2}^{-1}4s)$ core-excited state interacting with a metal surface. Figures 1 and 2 present the energy of the 4*s* electron in the $\mathrm{Ar}(2p_{3/2}^{-1}4s)$ state, E_{4s}, referred to the vacuum level and the corresponding RCT rate Γ_{RCT}, for a single Ar atom in front of the surface as functions of the Ar-surface distance. Both the cases of a free-electron metal and of a Cu(111) surface are considered. The distances are measured from the surface image plane. The adsorption distance in the Ar/Cu(111) system is equal to $4.73a_0$ from the surface image plane, and the analysis of the $\mathrm{Ar}^*(2p_{3/2}^{-1}4s)$ properties as functions of the atom-surface distance is performed to illustrate the characteristics of the RCT process in this system. In this first study, designed to stress the differences between the RCT processes in the case of Cu(111) and free-electron metal surfaces, the effective V_{ee} potential is not included so that the width of the level corresponds to the rate of the monoelectronic RCT process.

The results in Figs. 1 and 2 for the Cu(111) case are obtained with the method outlined above in Sec. II. They are compared with results (not detailed here) obtained with an effective range description of the $\mathrm{Ar}^*(2p_{3/2}^{-1}nl)$ states associated with the coupled angular mode treatment of the

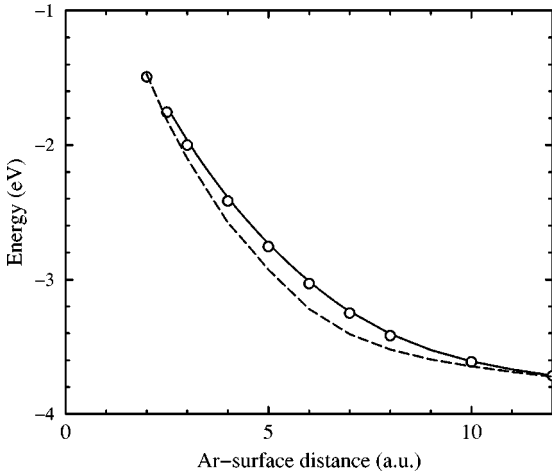

FIG. 1. Energy of the 4*s* electron in a core-excited $Ar^*(2p_{3/2}^{-1}4s)$ atom interacting with a metal surface as a function of the Ar–metal surface distance. A single Ar is present in front of the surface. The 4*s* electron energy is referred to the vacuum level. The distance is measured with respect to the image reference plane and the Ar adsorption distance is equal to $4.73a_0$. Dashed line: free-electron metal. Full line: Cu(111) surface with the WPP approach. Open circles: Cu(111) with the CAM approach.

adsorbate-substrate system (see, e.g., in Refs. 17 and 38). The two modelings of the electron interaction with the Ar^+ ion core are quite different, but nevertheless they lead to very similar results. The energies are practically equal and a small difference exists for the width. This gives confidence in the ability of these models to represent the $Ar^*(2p_{3/2}^{-1}4s)$ state.

The results for $Ar^*(2p_{3/2}^{-1}4s)$ adsorbed on a free-electron metal present the usual features for this kind of system.[22,23,30,38] The energy of the level increases as the atom approaches the surface, roughly following an image charge

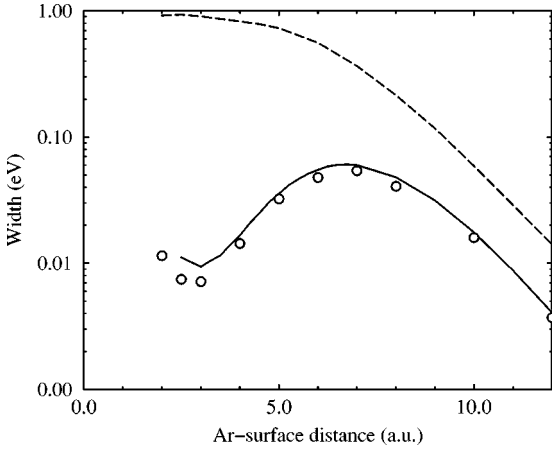

FIG. 2. Resonant charge transfer rate for the 4*s* electron in a core-excited $Ar^*(2p_{3/2}^{-1}4s)$ atom interacting with a metal surface as a function of the Ar–metal surface distance. A single Ar is present in front of the surface. The distance is measured with respect to the image reference plane and the Ar adsorption distance is equal to $4.73a_0$. Dashed line: free-electron metal. Full line: Cu(111) surface with the WPP approach. Open circles: Cu(111) with the CAM approach.

variation. At the adsorption distance, the 4*s* energy is located at −2.8 eV. The shift of the 4*s* energy from its position in the free Ar case is primarily due to the polarization of the metal, i.e., to electrical image interactions. As the atom approaches the surface, the level width increases roughly exponentially at large distances, reflecting the increasing overlap between atomic and metal wave functions. At small distances, the width saturates around 1 eV. At the adsorption distance, the level width is large, equal to 0.81 eV, corresponding to a very short lifetime of the state, 0.8 fs, against electron transfer to the surface. The results for the level energy in front of Cu(111) (Fig. 1) are quite comparable to those in front of a free-electron metal; however, the RCT widths (Fig. 2) differ considerably in the two systems. In particular, the width on Cu(111) is much smaller at small Ar-surface distances than on a free-electron metal surface. This difference is attributed to the effect of the *L* band gap of the Cu(111) surface [see discussions of the Cs/Cu(111) system in Refs. 30 and 54 and below]. The *Z* dependence of the $Ar^*(2p_{3/2}^{-1}4s)$ width is very similar to what has been found in calculations on the alkali/Cu(111) systems.[30,54] As *Z* decreases from very large distances, the RCT rate first increases exponentially following the variation of metal-atom wave function overlaps. Around $7a_0$, the rate starts to drop due to the onset of the polarization of the electronic cloud that enhances the band gap effect.[54] At the Ar adsorption distance the RCT rate on Cu(111) is equal to 0.03 eV, i.e., a factor of 27 smaller than on a free-electron metal surface, as a consequence of the band gap stabilization effect. The properties of the $Ar^*(2p_{3/2}^{-1}4s)$ state concerning the RCT process on metal surfaces are thus very similar to those of alkali metal atoms.

The difference between the free-electron and Cu(111) results can be further analyzed by looking at the excited electron wave function associated with the resonant $Ar^*(2p_{3/2}^{-1}4s)$ state in both cases. The wave function associated with a given resonance can be obtained via a Laplace transform of the propagated wave packet (see, e.g., Ref. 32). The corresponding electronic densities given by the square modulus of the resonant wave function for both surfaces are shown in Figs. 3(a) and 3(b) in the (ρ,z) plane. In the calculation of the resonant wave functions in Figs. 3(a) and 3(b), as well as for the other wave functions shown below, the multielectron interaction term has been omitted. Indeed, including it would result in the absorption of the electronic wave leaving Ar* and would thus hide the characteristics of the RCT which is shown below to be the dominating process in this system. These wave functions must then be considered as illustrations of the excited state wave functions and of the RCT decay. In Fig. 3(a), one recognizes the 4*s* orbital roughly centered on the Ar nucleus and an outgoing flux of electrons propagating in the metal along the surface normal, the *z* axis. This direction corresponds to the easiest tunneling direction for the electron on a free-electron metal, along which the potential barrier separating the metal and the atom is the smallest. In contrast, on Cu(111), since the 4*s* level energy lies inside the *L* band gap, there are no metal states propagating along the surface normal at this energy, and the electron can only be resonantly transferred to metal states with a momentum making a finite angle from the *z* axis or to

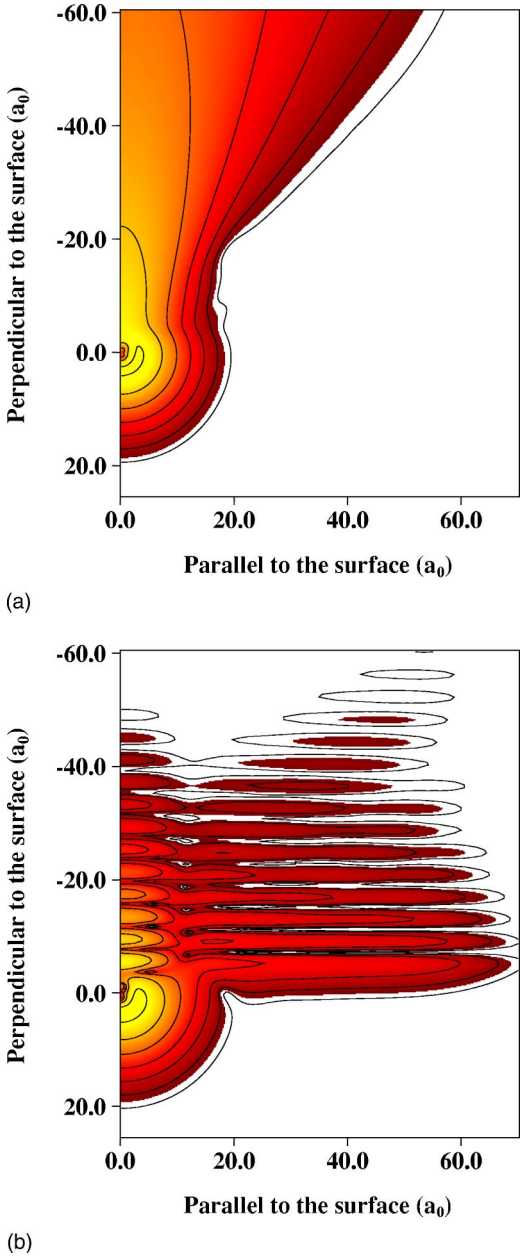

FIG. 3. (Color online) Contour plot of the resonant 4*s* wave function Ψ_R of a single core-excited $Ar^*(2p_{3/2}^{-1}4s)$ atom interacting with (a) a free-electron metal surface and (b) a Cu(111) surface. The Ar–metal surface distance is $4.73a_0$. $\mathrm{Log}(|\Psi_R|)$ is presented in cylindrical coordinates parallel and perpendicular to the surface. *z*, the coordinate normal to the surface, is positive in vacuum and the Ar atom center is located at $z=0$. The contour lines (thin full lines) correspond to 1.0 steps. The electron density decreases when going from light to dark gray. White corresponds to very small electron densities.

the 2D surface state continuum. The surface state wave function corresponds to an electron localized in the surface region and moving quasifreely parallel to the surface. This clearly appears in Fig. 3(b): the part of the resonance wave function along the *z* axis in Fig. 3(b) is an evanescent wave and the contributions from the two decay channels can easily be recognized. The outgoing flux parallel to the surface,

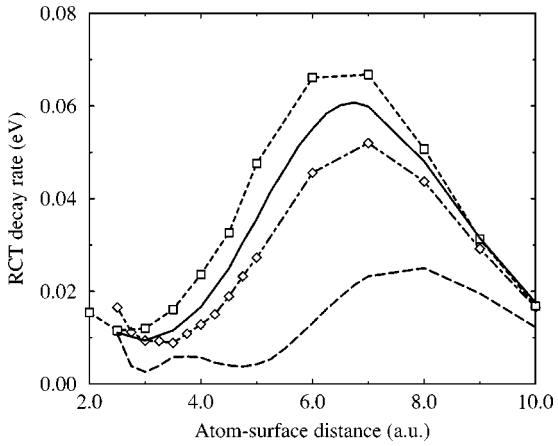

FIG. 4. Comparison of the RCT decay rate for the $Ar^*(2p_{3/2}^{-1}4s)$ core-excited-state atom interacting with a Cu(111) surface with earlier results for alkali atoms (K, Rb, and Cs) interacting with Cu(111). The RCT decay rate is presented as a function of the atom-surface distance, measured from the image reference plane. Full line: present results for $Ar^*(2p_{3/2}^{-1}4s)$. Results from Borisov *et al.* (Ref. 32) for the alkalis: open squares with dashed line, K(4*s*); open diamonds with dashed dotted line, Rb(5*s*); dashed line, Cs(6*s*).

close to it, corresponds to the decay into the surface state continuum. The outgoing flux into the metal along a direction making a finite angle with the surface normal corresponds to the decay rate into the 3D propagating states of Cu. This direction is associated with the smallest possible angle with the normal compatible with the resonance energy and the Cu band structure [see, e.g., the discussion in Ref. 37 in the case of H^-/Cu(111)]. One can also notice the very strongly distorted shape of the 4*s* orbital, resulting from the polarizing effect of the interaction with its own image and that of the Ar^+ ion core.

In order to quantitatively discuss the $Z+1$ approximation, we can compare the results in the $Ar^*(2p_{3/2}^{-1}4s)$/Cu(111) system to those for K(4*s*)/Cu(111). Figure 4 presents the RCT rate for $Ar^*(2p_{3/2}^{-1}4s)$/Cu(111) compared to earlier results for alkali adsorbates on[32,55] Cu(111) as functions of the atom-surface distance. Note that, for convenience, the various states are labeled with the name of the outer atomic orbital in the free-atom limit. As seen above, the quasistationary states close to the surface are strongly polarized and thus involve large mixings between the various orbitals of the free atom, so that the *ns* labeled states do not correspond to real *s* states. The adsorption distances of the alkali atoms and of Ar atoms on Cu(111) are quite different and so it is important for a valid test of the $Z+1$ approximation to be free of an adsorption distance effect. In the alkali adsorption region (distances in the $2.5a-3.5a_0$ range), all four systems (Ar*, K, Rb, and Cs) exhibit a very small RCT rate on Cu(111) in the 5–15 meV range, much smaller than on a free-electron metal surface where it typically amounts to 1 eV. However, quantitatively, the $Ar^*(2p_{3/2}^{-1}4s)$ state does not exactly correspond to K(4*s*); their widths differ by around 30–40 %. At the Ar adsorption distance ($4.73a_0$), the width of the Ar* state lies in between the K and Rb results.

TABLE II. Energy and charge transfer rate of the core-excited Ar*$(2p_{3/2}^{-1}4s)$ state of Ar adsorbed on a metal surface. Two different surfaces are shown for various Ar coverage on the surface: a free-electron metal surface and Cu(111). The energy E_{4s} of the excited 4*s* electron is given in eV with respect to vacuum. In the free-electron metal case, the charge transfer rate of the level corresponds to the resonant charge transfer process, Γ_{RCT}, which is dominant in that case. In the Cu(111) case, the charge transfer rate of the level is the total rate, Γ_T, sum of the rate corresponding to the resonant charge transfer process, Γ_{RCT}, and that for the effect of inelastic electron-electron interactions, Γ_{ee}. The charge transfer time is the inverse of the decay rate.

Coverage	Energy E_{4s} (eV)	RCT rate Γ_{RCT} (meV)	Total rate $\Gamma_T=\Gamma_{\mathrm{RCT}}+\Gamma_{ee}$	Charge transfer time τ ($\tau=1/\Gamma$) (fs)
		Ar*$(2p_{3/2}^{-1}4s)$ on a free-electron metal surface		
Single atom	−2.80	810		0.8
1 ML	−2.284	600		1.1
2 ML Ar* in inner layer	−1.67	1100		0.6
2 ML Ar* in outer layer	−2.738	36		18
		Ar*$(2p_{3/2}^{-1}4s)$/Cu(111)		
Single atom	−2.646	30		22
1 ML	−2.237	48	54 meV	12
2 ML Ar* in inner layer	−1.638		78 meV	8.5
2 ML Ar* in outer layer	−2.709		2.5 meV	260
3 ML Ar* in inner layer	−1.591		82.5 meV	8
3 ML Ar* in middle layer	−2.201		6.1 meV	107
3 ML Ar* in outer layer	−2.861		8.6×10^{-5} eV	7700

Roughly, one could say that, as far as the RCT rate is concerned, the Ar* state resembles Rb(5*s*) as much as K(4*s*). However, going back to one of the objectives of this work, the search for a band gap effect on the RCT process, one can conclude that the $Z+1$ approximation is at a quasiquantitative level in the present system.

IV. CORE-EXCITED Ar*$(2p_{3/2}^{-1}4s)$ ATOM INSIDE A LAYER ADSORBED ON A METAL

A. One monolayer Ar on a metal

We now consider the case of a core-excited Ar*$(2p_{3/2}^{-1}4s)$ atom inside a single monolayer of Ar adsorbed on a metal surface. The corresponding results are shown in Table II. The presence of the Ar neighbors significantly alters the energy of the level and the dynamics of the RCT process, but without modifying the large quantitative difference between the free-electron metal and Cu(111) surfaces.

For both metal surfaces, the energy of the level goes up by around 0.4–0.5 eV as an effect of the Ar layer. However, the change in the RCT rate is opposite on the two surfaces. The effect of the Ar neighbors on the E_{4s} energy and on the corresponding Γ_{RCT} can be understood as the result of the polarization of the Ar neighbours in the layer associated with the confinement of the 4*s* wave function due to the Ar neighbors. Indeed, the 4*s* level is located inside the bulk Ar band gap. When adsorbed on a metal surface and reduced to a single monolayer thickness, the Ar conduction band is strongly modified (see the discussion in Ref. 46). However, the 4*s* level is still in an energy range where propagation inside the Ar layer occurs only via tunneling. The 4*s* wave function cannot spread fully in space parallel to the surface as it does in the single adsorbed Ar case [see Figs. 3(a) and 3(b)] and it is repelled by the Ar neighbors. These effects can be easily seen on the wave function of the 4*s* resonance shown in Figs. 5(a) and 5(b) for 1 ML coverage in the free-electron and Cu(111) metal surface cases.

Figure 5(a) presents the wave function for a free-electron metal surface in the (ρ,z) plane, which contains one of the nearest Ar neighbors of the Ar*. The Ar* is centered at the origin of coordinates. One can recognize on the $z=0$ axis the effect of a nearest neighbor as a double lobe structure. The shape of the structure can be interpreted as the effect of the orthogonality of the 4*s* excited orbital on the core levels of the effective Ar potential. The main effect comes from the *p* core level with a smaller one from the deeper *s* level. One can connect the double lobe shape of the perturbation of the 4*s* wave function to the shape of the *p* core level wave function. Interestingly, one can see that this *p*-like structure is oriented toward the center of the electronic cloud and not toward the center of the Ar*, confirming this as the effect of the overlap between the 4*s* wave function and the *p* core level. The effect of a more distant Ar atom in the layer, located at twice the nearest distance, is also visible in the plane of the figure, although it is much fainter, due to the localization of the 4*s* orbital. This illustrates the convergence of the present calculation with the included in the calculation. Figure 5(b) shows a very similar effect in the case of the Cu(111) surface. One can see that difference between Figs. 5(a) and 5(b) concerns the electron transfer into the metal bulk; this difference is very similar to the one between Figs. 3(a) and 3(b). Indeed, this difference comes from the *L* band gap, a property of the Cu bulk crystal that is not modified by the presence of an Ar overlayer. In particular, one still

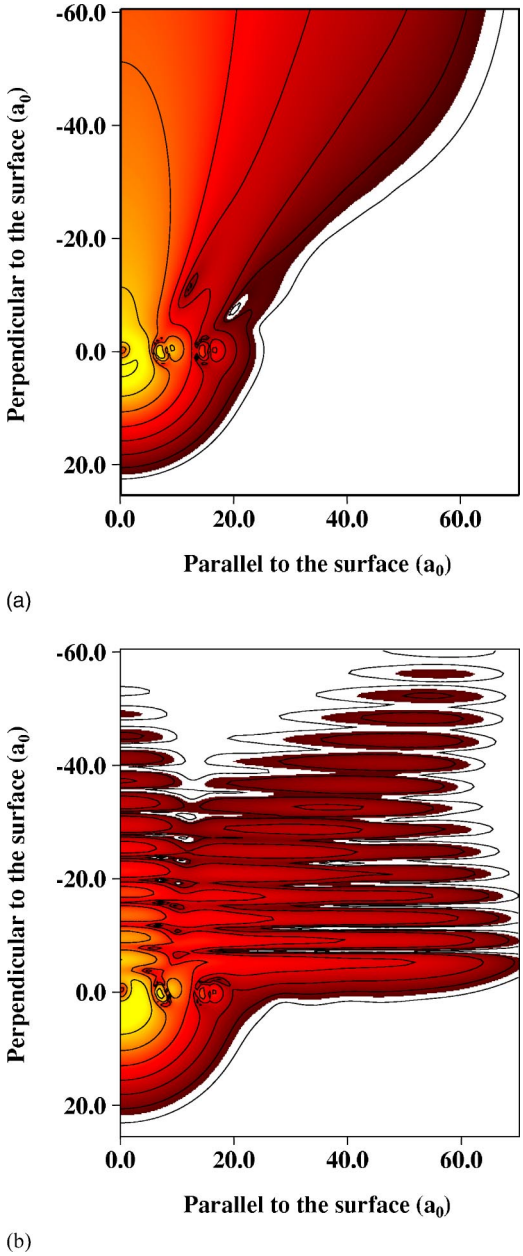

FIG. 5. (Color online) Contour plot of the resonant *4s* wave function Ψ_R of a core-excited $Ar^*(2p_{3/2}^{-1}4s)$ atom in the case of 1 ML of Ar adsorbed on (a) a free-electron metal surface and (b) a Cu(111) surface. The Ar–metal surface distance is $4.73a_0$. $\mathrm{Log}(|\Psi_R|)$ is presented in cylindrical coordinates parallel and perpendicular to the surface. *z*, the coordinate normal to the surface, is positive in vacuum and the Ar atom center is located at $z=0$. The contour lines (thin full lines) correspond to 1.0 steps. The electron density decreases when going from light to dark gray. White corresponds to very small electron densities.

recognizes the outgoing fluxes into the two decay channels of the resonance: 3D propagating bulk states and 2D surface states [one can stress that a Shockley surface state exists in the Ar/Cu(111) system;[56] it appears shifted compared to the clean Cu case but is not destroyed by the adsorbate layer].

The increase of the E_{4s} energy comes from two effects acting in the same direction: polarization of the Ar layer and confinement of the wave function. The E_{4s} energy measured with respect to vacuum is obtained as the energy difference between the system with an Ar* in the layer and the system with an Ar^+ in the layer. The latter includes the polarization of the layer and this leads to an increase of E_{4s}. As for confinement, it is visible in Fig. 5 where one can see that the 4*s* orbital overlaps the nearest Ar neighbors, so that the space available for the 4*s* electron is smaller than in the single adsorbed case, leading to an increase of E_{4s}. An estimate of the relative importance of these two effects can be obtained from the polarization energy of the Ar layer by the Ar+ ion. For 1 ML, it amounts to 0.19 eV, to be compared to the 0.4–0.5 eV change of E_{4s}.

TABLE III. Convergence of the properties of the $Ar^*(2p_{3/2}^{-1}4s)$ state in the case of 1 ML Ar adsorbed on Cu(111) as a function of the number of Ar atoms actually included in the calculation. The energy E_{4s} of the level is given in eV with respect to the vacuum level. The decay rate given in eV corresponds to the resonant transfer of the 4*s* electron into Cu.

	E_{4s} (eV)	RCT rate (eV)
1 hexagon, 6 atoms	−2.253	0.053
2 hexagons, 18 atoms	−2.238	0.0475
3 hexagons, 36 atoms	−2.237	0.048

As for the RCT decay rate, one can see in Fig. 5(b) that the polarized shape of the 4*s* orbital is modified by the presence of the Ar neighbors. Since the band gap effect is strongly enhanced by the polarization of the 4*s* orbital (see the discussion in Ref. 54), partly disturbing this polarization results in a drop of the band gap effect, i.e., to the observed increase of the RCT rate on Cu(111) due to the Ar neighbors. On the free-electron metal surface, the importance of polarization is weaker and one simply has the effect that the 4*s* electron is mainly located above the Ar layer in vacuum and its tunneling into the metal is slightly hindered on the edges by the Ar neighbors, resulting in a slight decrease of the RCT rate.

The convergence of the $Ar^*(2p_{3/2}^{-1}4s)$ state properties (energy and RCT rate) with the number of Ar atoms actually included in the layer has been tested by comparing the results obtained with different numbers of Ar atoms in the case of one monolayer on Cu(111): 6, 18, or 36 atoms corresponding to the first, second, and third hexagons surrounding a given site in a fcc (111) plane. The corresponding results are summarized in Table III. They show the very fast convergence of the results; typically, including only up to the second hexagon surrounding a given site is enough to reach convergence. This confirms the visual conclusion drawn from the perturbation of the distant Ar atoms on the 4*s* wave function (Fig. 5) and, again, is a direct consequence of the finite size of the 4*s* orbital. One can also stress that the long-range interaction between the core-excited Ar atom and the other Ar atoms in the layer (polarization of the distant atoms by the Ar*) is weak. In the present approach, the Ar* is polarized, but the corresponding dipole is screened by the presence of the metal surface, so that only higher order multipole terms are present for distant Ar atoms in the layer.

Similarly to the alkali/Cu(111) systems, since the RCT process is weak on the Cu(111) surface, one must consider a higher order decay process for the transfer of the 4*s* electron in bulk Cu: the effect of the inelastic scattering of the 4*s* electron with the metal bulk electrons. Using the effective complex potential approach, $-iV_{ee}$, we estimated the decay rate for this process at 6.3 meV for the $Ar^*(2p_{3/2}^{-1}4s)$ state at the equilibrium distance. Although not negligible in this case, it is much smaller than the RCT contribution of 47 meV. The smaller importance of the multielectron effects in the $Ar^*(2p_{3/2}^{-1}4s)/Cu(111)$ compared to the alkali metal Cu(111) is attributed to the larger adsorption distance, which decreases the excited state–bulk overlap. As a conclusion for the *e-e* interaction effect, it is present in this system, but it only slightly influences the quantitative results on Cu(111). Below, the discussions of the multilayer case and of the variation of the charge transfer rate with the Ar* environment are based on the variations of the RCT process, the multielectron process contribution to the charge transfer being smaller. However, the total charge transfer rates for these two systems ($\Gamma_T=\Gamma_{RCT}+\Gamma_{ee}$, in column 4 of Table II) have been evaluated with the multielectron process taken into account.

B. Ar multilayers on a metal surface

Table II presents a comparison between the results for the $Ar^*(2p_{3/2}^{-1})4s$ state properties for various Ar coverages of the surfaces [free-electron metal and Cu(111) surfaces]. In the case of multilayer coverage, all the Ar sites in the layer are not equivalent. In Table II and below, we label "inner" the Ar in the layer directly in contact with the metal substrate and "outer" the Ar in the layer located at the vacuum interface. For 3 ML, the intermediate layer is called "middle." The energies and charge transfer rates of the 4*s* level are quite different for the different positions in the layer. The site dependence is qualitatively the same for the two metal substrates. As a general remark on the results in Table II, one can say that the energy is lower and the decay rate is much lower when moving from the inner to the outer position in the layer.

To analyze and illustrate the effects on the RCT rate, let us look at the wave function of the 4*s* resonant orbital in the case of 2 ML Ar/Cu(111). The calculation is made without the V_{ee} term. Figure 6 presents the 4*s* wave function in the case of an inner Ar. The relative positions of Ar* and Cu are identical to those in the 1 ML case; the difference between the two sets of results (Table II) are then due entirely to the effects of the Ar neighbors in the second layer. Figure 6 presents the square modulus of the wave function in a plane ρ,z perpendicular to the surface that contains the centers of the Ar* and of one of the Ar in the outer layer. The RCT decay of the 4*s* electron into Cu is similar to the cases discussed above: one recognizes on the figure the evanescent wave located around the $\rho=0$ axis and the outgoing flux into the metal that occurs only beyond a certain angle from the normal. The nearest neighbors of Ar* in the inner layer are not centered in the plane of the figure, and their effect does not appear in it. In the plane of the figure, the first neighbor

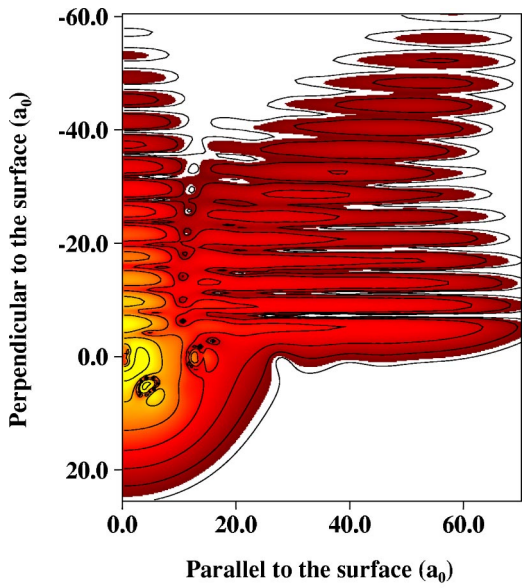

FIG. 6. (Color online) Contour plot of the resonant 4*s* wave function Ψ_R of a core-excited $Ar^*(2p_{3/2}^{-1}4s)$ atom in the case of 2 ML of Ar adsorbed on a Cu(111) surface. The core-excited Ar* is located in the inner Ar layer, the closest to the metal. Log($|\Psi_R|$) is presented in cylindrical coordinates parallel and perpendicular to the surface. *z*, the coordinate normal to the surface, is positive in vacuum and the Ar atom center is located at $z=0$. The contour lines (thin full lines) correspond to 1.0 steps. The electron density decreases when going from light to dark gray. White corresponds to very small electron densities.

in the inner layer is located at a distance equal to $\sqrt{3}$ times the nearest distance in the layer. Its effect, although visible, is smaller than the one resulting from the nearest neighbors that was visible in Fig. 5. In the plane shown in Fig. 6, the nearest neighbor belongs to the outer layer and it is located well inside the 4*s* electronic cloud as it results from the polarization of the 4*s* orbital [see, e.g., Fig. 3(b) or Fig. 5(b)]. This Ar neighbor is very efficient in confining the 4*s* orbital; it disturbs the polarization of the 4*s* orbital and the RCT-blocking effect of the Cu(111) band gap. Thus, the first neighbors in the outer layer are responsible for the larger 4*s* decay rate in the inner 2 ML case, 78 meV, compared to the 54 meV in the 1 ML case (see Table II). As for the energy of the 4*s* level, the polarization of the Ar in the outer layer as well as the confinement of the 4*s* orbital by the second layer (see Fig. 6) are both acting in the same direction: they lead to the increase of the level energy seen in Table II. The above effects discussed in the Cu(111) case and accounting for the differences between the 1 ML and 2 ML inner cases are also active in the case of a free-electron metal surface and similarly account for the differences seen in Table II.

Let us now consider the case of the Ar* located in the outer layer. First, compared to the inner layer case, the Ar*-surface distance is larger and from the results on a single Ar* atom in front of the surface (see Figs. 1 and 2), one could expect a larger RCT rate and a lower energy than for the inner Ar case. The effect of the adsorption height on the energy (see Table II) corresponds to this expectation; the

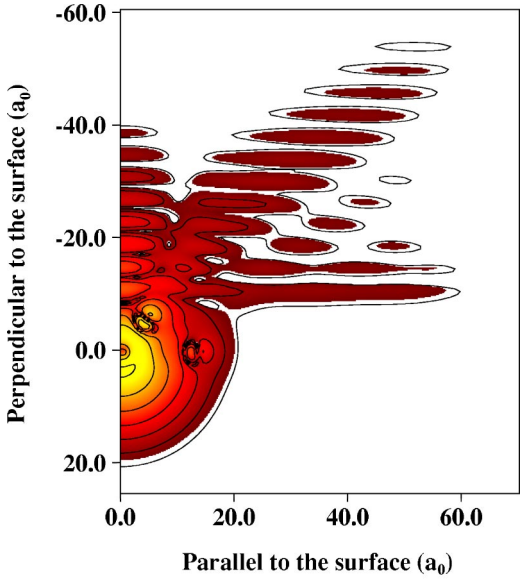

FIG. 7. (Color online) Contour plot of the resonant 4*s* wave function Ψ_R of a core-excited $Ar^*(2p_{3/2}^{-1}4s)$ atom in the case of 2 ML of Ar adsorbed on a Cu(111) surface. The core-excited Ar* is located in the outer Ar layer, the furthest away from the metal. $\mathrm{Log}(|\Psi_R|)$ is presented in cylindrical coordinates parallel and perpendicular to the surface. *z*, the coordinate normal to the surface, is positive in vacuum and the Ar atom center is located at $z=0$. The contour lines (thin full lines) correspond to 1.0 steps. The electron density decreases when going from light to dark gray. White corresponds to very small electron densities.

Ar layer polarization and confinement effects do not modify the relative position of the inner and outer layer energies. The situation is different for the level decay rate. To discuss this aspect, Fig. 7 presents the square modulus of the 4*s* wave function in a plane ρ,z perpendicular to the surface that contains the centers of the Ar* and of one of the Ar nearest neighbors in the inner layer. The polarization of the 4*s* orbital is now similar to the one found in the 1 ML case and is not much perturbed by the second layer. However, the decay of the 4*s* electron implies that the electron crosses the inner Ar layer. This is difficult since Ar is an insulator and the 4*s* electron lies within its forbidden band gap. Rare gas adsorbed layers have insulator properties, even at the monolayer level.[45,46,57–59] This leads to a significant drop of the RCT rate as compared to the situation where the Ar* atom is directly adsorbed on the metal. It explains the drop of the RCT rate by a factor of 30 between the inner and outer layers.

As seen in Table II, the free-electron metal case is very similar to the Cu(111) case: it exhibits the same striking difference between the inner and outer Ar* positions. However, one can see that the effect of the projected band gap is still visible in the outer layer, the RCT rates being significantly lower on the Cu(111) substrate.

The case of 3 ML Ar adsorbed on Cu(111) presents the same qualitative features, but more pronounced (see Table II). For the inner Ar* position, the presence of a third outer layer further enhances the effects already seen in the 2 ML case. However, one can see that the effect of the third layer is smaller than that of the second, as expected from its larger distance to the Ar* atom. For an Ar* located in the middle layer of the 3ML system, the inner layer (closest to the surface) plays the role of a dielectric spacer layer, the same as for an Ar* located in the outer layer of the 2 ML system. Thus the RCT rate is strongly reduced in the middle layer of the 3 ML system as compared to the Ar* located in the inner layer of the 3 ML system or to the Ar* in the 1 ML system. On the other hand, it appears that the RCT rate in the middle layer of the 3 ML system is larger than in the outer layer of the 2 ML system. This is due to the perturbation of the 4*s* electronic cloud by the Ar atoms in the outer layer of the 3 ML system. This confinement effect was already observed and discussed in the case of the inner layer in the 2 ML system and accounts for the decay rate difference.

The most striking effect in the 3 ML system concerns the RCT rate in the outer layer, which becomes extremely weak. The charge transfer time in this case reaches the few picoseconds range. The RCT rate for the outer position in the 3 ML case is around a factor of 30 smaller than the rate in the outer 2 ML case, i.e., an effect comparable to that observed between 1 ML and 2 ML. This is again attributed to the insulator properties of solid Ar and the factor of 30 can simply be interpreted as the typical value for the inverse of the transmission probability of an electron at the 4*s* level energy through a monolayer of Ar. One can see that this effect is stronger than the one observed for the image states in the Ar/Cu(100) system, in which the image state decay is also hindered by the transmission of the image state electron through the Ar layer.[45,46] The different magnitude of the Ar transmission effect is attributed to the different energies of the electron tunneling through the Ar layer in the two systems. The energy is lower in the case of the $Ar^*(2p_{3/2}^{-1}4s)$ state and thus lower in the Ar band gap, accounting for a lower transmission probability. This aspect confirms the discussion of the differences between the various image states in the Ar/Cu(100) system.[46]

V. DISCUSSION AND COMPARISON WITH EXPERIMENTAL DATA

A. Energy and charge transfer rate

The $Ar^*(2p_{3/2}^{-1}4s)$ state has been recently studied experimentally in the case of 1 ML Ar adsorbed on Cu(111),[14] using the core clock method. The 4*s* level has been found at 2.9 ± 0.2 eV above the Fermi level with a charge transfer time τ (inverse of the charge transfer rate) equal to 7 fs. These have to be compared with the present results of 2.71 eV and 12 fs. The agreement on the energy is quite satisfying. For the charge transfer time, one should notice that the experimental result on Cu(111) is significantly longer than what is predicted for a free-electron metal (around 1 fs), confirming the role of the Cu(111) projected band gap in blocking the charge transfer. The experimental value is, however, shorter than the present theoretical result. This discrepancy might be due to the approximations involved in the present modeling. Another origin could be the assumption in

the experimental procedure of a core hole decay time unaffected by the adsorption.

The charge transfer time for the $Ar^*(2p_{3/2}^{-1}4s)$ state has also been measured for other systems. In the 1 ML Ar on Ag(111) system, the measured charge transfer time is around 7 fs,[14] as on Cu(111), consistently with the similarity of the electronic structure of these two systems with projected band gaps roughly located in the same energy region. For 1 ML Ar on other noble metals, Sandell *et al.*[8] reported a much smaller charge transfer time, around 1 fs for Ag(110) and Cu(100) substrates. A fast charge transfer is not surprising on the Ag(110) surface, which does not exhibit a projected band gap along the surface normal at the 4*s* level energy and should then qualitatively behave similarly to a free-electron metal surface. As for Cu(100), it exhibits a projected band gap along the surface normal in the right energy range and one should expect a charge transfer time longer than on a free-electron metal. However, the 4*s* level is lower in the surface-projected band gap on Cu(100) than on Cu(111), leading to a weaker band gap blocking effect on Cu(100) than on Cu(111). This situation is then similar to what has been found in the case of alkali atoms on the various Cu surfaces (see the discussion in Ref. 31). Results are also available for Ni(111) (τ around 5 fs), Pt(111) (τ around 5 fs), and Ru(0001) (τ around 1.5 fs). In these systems, the 3*d* levels of the substrate could play a role and modify the blocking of the charge transfer due to the *sp* band. The Ar/Ru(0001) system is currently under investigation.[61]

B. Ar multilayers on metals

In the case of a Ru(0001) substrate, experiments were also performed for multilayers involving Ar and Xe layers.[6,12,13] These showed the same qualitative variations of the charge transfer time τ as found here for Ar multilayers. First, when 1 ML of Xe is put underneath 1 ML of Ar (Ar/Xe/Ru system), τ rises from 1.5 fs to 12 fs,[6,12,13] i.e., one observes exactly the same insulator effect of a rare gas layer as discussed above for Ar, although weaker. This difference in the relative insulating properties of Ar and Xe can be attributed to the lower energy position of the conduction band bottom in Xe than in Ar, which makes the transmission probability through Ar smaller than through Xe (see, e.g., the discussion in Ref. 46). In the Ar/Ar/Xe/Ru system, τ for the inner Ar layer is found equal to 8 fs, i.e., a factor of 1.5 shorter than in the Ar/Xe/Ru system.[6,12] This is the same effect as found here and discussed above as the outer Ar layer perturbing the Ar 4*s* orbital in the inner layer. Finally, for the Ar* located in the outer layer in the Ar/Ar/Xe/Ru system, experimental limitations made impossible the accurate determination of τ, which can only be said to be longer than 50 fs.[6,12,13] Again, this is the same layer thickness dependence as found here, due to the low electron transmission probability of an Ar layer at the 4*s* energy.

C. Energy dependence of the charge transfer time

A surprising feature has been found in the experimental studies using the core hole clock method. The charge transfer time τ was derived from the relative importance of the charge transfer and of the core hole decay channels in the decay of the $Ar^*(2p_{3/2}^{-1}4s)$ state. The sharing ratio between these two channels was found to vary with the energy across the Ar* line shape, apparently pointing at an energy dependence of the charge transfer time. τ was found to increase with the excitation energy in the case of Cu(111), Ag(111), and Ni(111) substrates[14] and to maximize at the level position in the case of a Pt(111) substrate.[11] The variation is quite significant, around a factor 2–3 across the resonance profile for Cu(111). Various possible origins for this variation have been discussed.[12,14,60] Within the present approach, we can look for an energy dependence of the charge transfer process. A first possibility, already suggested, comes from the energy dependence of the adsorbate-substrate coupling matrix element, which could be enhanced by the blocking effect of the Cu(111) projected band gap. The present WPP result yields the density of states projected on the initial wave packet and a strong energy dependence of the charge transfer coupling should appear as an asymmetric line shape for the 4*s* level peak in the projected density of states. Detailed checks of this line shape did not reveal any significant asymmetry, so that we can rule out in the present system a strong effect of an energy dependence of the charge transfer coupling.

In Ref. 14, the experimental resonance profile of the $Ar^*(2p_{3/2}^{-1}4s)$ state as a function of the excitation energy is highly asymmetric, extending farther out below the resonance than above. This suggests the possibility of inhomogeneous broadening, different positions of the Ar* in the system leading to different x-ray absorption energies and

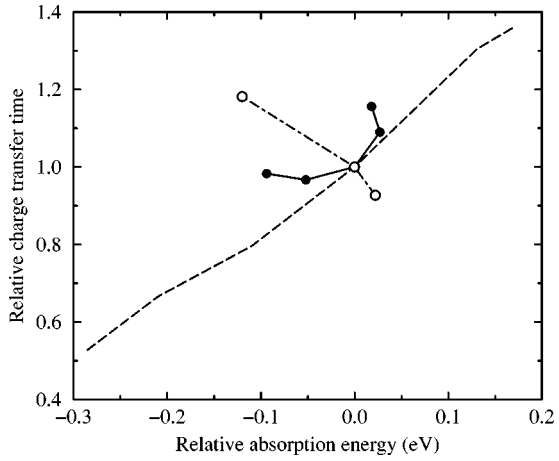

FIG. 8. Correlation between the excitation energy of the $Ar^*(2p_{3/2}^{-1}4s)$ core-excited state and the charge transfer time to the metal of the 4*s* electron. The experimental results of Föhlisch *et al.* Ref. 14 [1 ML Ar/Cu(111)] are shown by the dashed line. The experimental excitation energy is plotted with respect to the center of the absorption line whereas the charge transfer time is presented relative to its value at the center of the absorption line. The symbols show the present theoretical results for a system in which the Ar* is displaced with respect to its equilibrium position in a 1 ML Ar layer on a metal surface. Full circles and full lines: Cu(111) surface. Open circles and dash-dotted line: free-electron metal surface. For both surfaces, the theoretical results are plotted with respect to the excitation energy and charge transfer time for the Ar* at its equilibrium position.

different charge transfer times. To test this possibility, we performed a few calculations with the core-excited atom slightly displaced from its equilibrium position in the layer, while all the other Ar atoms remain unchanged. We determined the energy of the level and the charge transfer time in these positions and looked for the correlation between these two results. For this, the energy cannot be the 4*s* energy discussed above but rather the x-ray absorption energy. The latter was approximated by

$$E_{\mathrm{abs}} = E_{\mathrm{abs}}^{\mathrm{at}} - E_{4s}^{\mathrm{at}} + E_{4s} - E_{\mathrm{pol}}, \tag{13}$$

where E_{abs} and $E_{\mathrm{abs}}^{\mathrm{at}}$ are the x-ray absorption energies in the adsorbate system and in the free atom, and E_{4s} and E_{4s}^{at} are the 4*s* electron energies with respect to vacuum in the adsorbate system and in the free atom. E_{pol} is the polarization energy of the Ar layer by the Ar^+ core. The latter is calculated by the same method as outlined above for the electron–Ar layer interaction potential. Expression (13) introduces a further approximation in the study, it assumes that the x-ray absorption line shift only comes from the one-electron energy change.

Figure 8 shows the results for the core-excited Ar* displaced perpendicular to the surface from its equilibrium adsorption height. The maximum displacement on the figure is $\pm 1a_0$. This kind of displacement was chosen since one can expect a variation of the charge transfer rate with the adsorption distance (see Fig. 2); in addition, it does not decrease the symmetry of the system, which is a favorable aspect from the computer time point of view. The results are presented with respect to the absorption energy and the charge transfer time at the equilibrium position [$E_{\mathrm{abs}} - E_{\mathrm{abs}}$(equilibrium) and $\tau_{\mathrm{CT}}/\tau_{\mathrm{CT}}$(equilibrium)] and they are compared to the experimental results of Föhlisch *et al.*[14] It appears that the correlation between E_{abs} and τ is opposite for Cu(111) and free-electron metal surfaces. The correlation found here on the Cu(111) substrate is similar to the one found experimentally: the charge transfer time increases when the energy increases. However, the total width of variation is much smaller than the one found experimentally. The four points for the Cu(111) surface correspond to *z* shifts of the Ar* by $\pm 0.4a_0$ and $\pm 1a_0$. Assuming they are equally probable and that the x-ray absorption strength would be the same for all of them, from Fig. 8 one can predict an asymmetric line shape for the absorption line on the Cu(111) substrate, broader on the low energy side, as observed by Föhlisch *et al.*[14] However, the effect seen in Fig. 8 is smaller than observed experimentally, although the displacement of the Ar* is large. One can then conclude that, although in the right direction, the effect of inhomogeneities of the layer seems to be too weak to account for the observations. Nevertheless, one should stress that only one simple case of layer inhomogeneities has been investigated. In addition, defects in the Ar layer adsorbed on the metal could also lead to an apparent energy dependence of the charge transfer rate, similarly to the effect of the Ar displacement discussed here.

VI. CONCLUDING SUMMARY

We have reported on a parameter-free study of the energy and charge transfer decay rate of the core-excited $\mathrm{Ar}^*(2p_{3/2}^{-1}4s)$ atom adsorbed on Cu(111) and free-electron metal surfaces. The main results follow.

The charge transfer rate of the 4*s* electron and the metal substrate is quite different on a free-electron metal and on a Cu(111) surface. The presence of the Cu *L* band gap results in an efficient blocking of the resonant electron transfer process, leading to very long charge transfer times for the 4*s* electron on Cu(111). On the Cu(111) surface, the charge transfer induced by multielectron interactions is found to be significantly weaker than is the resonant charge transfer.

The blocking effect of the Cu(111) projected band gap is similar for the $\mathrm{Ar}^*(2p_{3/2}^{-1}4s)$ state and for the alkali metal atoms. This confirms the validity of the so-called $Z+1$ approximation, as well as the validity of the criteria discussed in Ref. 54 for the appearance of the band gap blocking effect. The $Z+1$ approximation is nevertheless not completely quantitative, differences being found between the $\mathrm{Ar}^*(2p_{3/2}^{-1}4s)$ and K(4*s*) states.

The energy and the decay rate of the $\mathrm{Ar}^*(2p_{3/2}^{-1}4s)$ state appear to be much influenced by the presence of Ar neighbors. Three different effects have been identified: (i) the polarization of the Ar neighbors by the ion core and electron fields that modifies the potential felt by the 4*s* electron; (ii) the confinement of the 4*s* electron wave function by the Ar neighbors; the 4*s* wave function cannot expand freely in space leading to an energy increase as well as to a modification of the polarization of the orbital; and (iii) the insulator character of a very thin Ar layer which is already present even in a single monolayer; the transmission probability of a 4*s* electron through an Ar layer is very weak, leading to very long charge transfer times in the case of Ar* located in the outer layer of a multilayer system.

On Cu(111) surfaces for 1–3 ML coverages, the charge transfer time is found to be longer than the decay time of the core hole in Ar*. However, with the exception of the outer layers in the 2 and 3 ML coverages, the two rates are of comparable magnitude, which allows for the measurements of the corresponding branching ratios and thus the use of the core hole clock method in this system.[14]

The above features of the charge transfer were also found in experimental studies of Ar physisorbed on Cu(111) surfaces as well as on other surfaces. In particular, a long charge transfer time has been reported for the Cu(111) surface,[14] confirming the *L* band gap effect found here. Strong effects of the Ar neighbors on the 4*s* charge transfer time have been observed,[13] similarly to the present theoretical findings.

An interpretation has been proposed for the excitation energy dependence of the charge transfer time observed experimentally,[14] based on the existence of inhomogeneities in the Ar layer. The present study performed for geometries in which the Ar* atom is displaced along the surface normal, while the other Ar atoms are kept at their equilibrium positions, predicts a correlation between the excitation energy and the charge transfer rate in the same direction as that observed experimentally. At the same time, this effect seems

too weak to account for the experimental findings. This could invalidate the proposed interpretation or point to the need of other defect geometries that could account for the experimental observations. Further work is needed to reach a definitive statement.

ACKNOWLEDGMENTS

Enlightening discussions with P. Lablanquie about the $Ar^*(2p_{3/2}^{-1}4s)$ state and with W. Wurth and A. Föhlisch about their results on Ar*/metal are gratefully acknowledged.

[1] G. S. Brown, M. H. Chen, B. Crasemann, and G. E. Ice, Phys. Rev. Lett. **45**, 1937 (1980).
[2] A. Kivimäki, A. Naves de Brito, S. Aksela, H. Aksela, O.-P. Sairanen, A. Ausmees, S. J. Osborne, L. B. Dantas, and S. Svensson, Phys. Rev. Lett. **71**, 4307 (1993).
[3] O. Björneholm, A. Nilsson, A. Sandell, B. Hernnäs, and N. Mårtensson, Phys. Rev. Lett. **68**, 1892 (1992).
[4] M. Ohno, Phys. Rev. B **50**, 2566 (1994).
[5] A. Sandell, O. Hjortstam, A. Nilsson, P. A. Brühwiler, O. Eriksson, P. Bennich, P. Rudolf, J. M. Wills, B. Johansson, and N. Mårtensson, Phys. Rev. Lett. **78**, 4994 (1997)
[6] C. Keller, M. Stichler, G. Comelli, F. Esch, S. Lizzit, D. Menzel, and W. Wurth, Phys. Rev. B **57**, 11 951 (1998).
[7] C. Keller, M. Stichler, G. Comelli, F. Esch, S. Lizzit, W. Wurth, and D. Menzel, Phys. Rev. Lett. **80**, 1774 (1998).
[8] A. Sandell, P. A. Brühwiler, A. Nilsson, P. Bennich, P. Rudolf, and N. Mårtensson, Surf. Sci. **429**, 309 (1999).
[9] H. Petek and S. Ogawa, Prog. Surf. Sci. **56**, 239 (1997).
[10] D. A. Shaw, G. C. King, F. H. Read, and D. Cvejanovic, J. Phys. B **15**, 1785 (1982).
[11] O. Karis, A. Nilsson, M. Weinelt, T. Wiell, C. Puglia, N. Wassdahl, N. Mårtensson, M. Samant, and J. Stöhr, Phys. Rev. Lett. **76**, 1380 (1996).
[12] C. Keller, M. Stichler, G. Comelli, F. Esch, S. Lizzit, D. Menzel, and W. Wurth, J. Electron Spectrosc. Relat. Phenom. **93**, 135 (1998).
[13] W. Wurth and D. Menzel, Chem. Phys. **251**, 141 (2000).
[14] A. Föhlisch, D. Menzel, P. Feulner, M. Ecker, R. Weimar, K. L. Kostov, G. Tyuliev, S. Lizzit, R. Larciprete, F. Hennies, and W. Wurth, Chem. Phys. **289**, 107 (2002).
[15] J. Los and J. J. C. Geerlings, Phys. Rep. **190**, 133 (1990).
[16] P. Nordlander and J. C. Tully, Phys. Rev. Lett. **61**, 990 (1988).
[17] D. Teillet-Billy and J. P. Gauyacq, Surf. Sci. **239**, 343 (1990).
[18] V. A. Ermoshin and A. K. Kazansky, Phys. Lett. A **218**, 99 (1996).
[19] F. Martin and M. F. Politis, Surf. Sci. **356**, 247 (1996).
[20] S. A. Deutscher, X. Yang, and J. Burgdörfer, Phys. Rev. A **55**, 466 (1997).
[21] P. Kürpick, U. Thumm, and U. Wille, Nucl. Instrum. Methods Phys. Res. B **125**, 273 (1997).
[22] A. G. Borisov, D. Teillet-Billy, and J. P. Gauyacq, Phys. Rev. Lett. **68**, 2842 (1992).
[23] A. G. Borisov, D. Teillet-Billy, J. P. Gauyacq, H. Winter, and G. Dierkes, Phys. Rev. B **54**, 17 166 (1996).
[24] S. B. Hill, C. B. Haich, Z. Zhou, P. Nordlander, and F. B. Dunning, Phys. Rev. Lett. **85**, 5444 (2000).
[25] N. D. Lang and A. R. Williams, Phys. Rev. B **18**, 616 (1978).
[26] M. Bauer, S. Pawlik, and M. Aeschlimann, Phys. Rev. B **55**, 10 040 (1997).
[27] M. Bauer, S. Pawlik, and M. Aeschlimann, Phys. Rev. B **60**, 5016 (1999).
[28] S. Ogawa, H. Nagano, and H. Petek, Phys. Rev. Lett. **82**, 1931 (1999).
[29] H. Petek, M. J. Weida, H. Nagano, and S. Ogawa, Science **288**, 1402 (2000).
[30] A. G. Borisov, A. K. Kazansky, and J. P. Gauyacq, Surf. Sci. **430**, 165 (1999).
[31] A. G. Borisov, J. P. Gauyacq, A. K. Kazansky, E. V. Chulkov, V. M. Silkin, and P. M. Echenique, Phys. Rev. Lett. **86**, 488 (2001).
[32] A. G. Borisov, J. P. Gauyacq, E. V. Chulkov, V. M. Silkin, and P. M. Echenique, Phys. Rev. B **65**, 235434 (2002).
[33] A. G. Borisov, A. K. Kazansky, and J. P. Gauyacq, Phys. Rev. B **64**, 201105(R) (2001).
[34] N. Lorente and R. Monreal, Surf. Sci. **370**, 324 (1997).
[35] E. V. Chulkov, I. Sarria, V. M. Silkin, J. M. Pitarke, and P. M. Echenique, Phys. Rev. Lett. **80**, 4947 (1998).
[36] O. Hjortstam, J. M. Wills, B. Johansson, and O. Eriksson, Phys. Rev. B **58**, 13 191 (1998).
[37] A. G. Borisov, A. K. Kazansky, and J. P. Gauyacq, Phys. Rev. B **59**, 10 935 (1999).
[38] J. P. Gauyacq, A. G. Borisov, and G. Raşeev, Surf. Sci. **490**, 99 (2001).
[39] P. J. Jennings, R. O. Jones, and M. Weinert, Phys. Rev. B **37**, 6113 (1988).
[40] E. V. Chulkov, V. M. Silkin, and P. M. Echenique, Surf. Sci. **437**, 330 (1999).
[41] L. Kleinman and D. M. Bylander, Phys. Rev. Lett. **48**, 1425 (1982).
[42] J. N. Bardsley, Case Stud. At. Phys. **4**, 299 (1974).
[43] G. C. King, M. Tronc, F. H. Read, and R. C. Bradford, J. Phys. B **10**, 2479 (1977).
[44] L. Avaldi, G. Dawber, R. Camilloni, G. C. King, M. Roper, M. R. F. Siggel, G. Stefani, and M. Zitnik, J. Phys. B **27**, 3953 (1994).
[45] D. C. Marinica, C. Ramseyer, A. G. Borisov, D. Teillet-Billy, J. P. Gauyacq, W. Berthold, P. Feulner, and U. Höfer, Phys. Rev. Lett. **89**, 046802 (2002).
[46] D. C. Marinica, C. Ramseyer, A. G. Borisov, D. Teillet-Billy, and J. P. Gauyacq, Surf. Sci. **540**, 457 (2003).
[47] K. Horn, C. Mariani, and L. Cramer, Surf. Sci. **117**, 376 (1982).
[48] M. A. Van Hove, W. H. Weinberg, and C. M. Chan, *Low Energy Electron Diffraction, Theory and Experiment* (Springer-Verlag, Heidelberg, 1986).
[49] P. M. Echenique, J. M. Pitarke, E. V. Chulkov, and A. Rubio, Chem. Phys. **251**, 1 (2000).
[50] M. D. Fleit and J. A. Fleck, J. Chem. Phys. **78**, 301 (1983).
[51] R. Kosloff, J. Phys. Chem. **92**, 2087 (1988).
[52] D. T. Colbert and W. H. Miller, J. Phys. Chem. **96**, 1982 (1992).
[53] A. G. Borisov, J. P. Gauyacq, and S. V. Shabanov, Surf. Sci. **487**, 243 (2001).
[54] J. P. Gauyacq, A. G. Borisov, G. Raşeev, and A. K. Kazansky,

Faraday Discuss. **117**, 15 (2000).
[55] A. G. Borisov (unpublished).
[56] F. Forster, G. Nicolay, F. Reinert, D. Ehm, S. Schmidt, and S. Hüfner, Surf. Sci. **532**, 160 (2003).
[57] D. F. Padowitz, W. R. Merry, R. E. Jordan, and C. B. Harris, Phys. Rev. Lett. **69**, 3583 (1992).
[58] A. Hotzel, K. Ishioka, E. Knoesel, M. Wolf, and G. Ertl, Chem. Phys. Lett. **285**, 271 (1998).
[59] M. Michaud, L. Sanche, C. Gaubert, and R. Baudoing, Surf. Sci. **205**, 447 (1988).
[60] Z. W. Gortel and D. Menzel, Phys. Rev. B **64**, 115416 (2001).
[61] D. Sanchez-Portal (private communication).